Journal of Morphological Sciences
J Morphol Sci
Brazilian Society of Anatomy

Original Article
J Morphol Sci 2026;43:114-125

Bone Repair Using Synthetic Porous Hydroxyapatite for Critical Defects in the Calvaria of *Rattus Norvegicus* (Wistar Lineage)

Marcella Dall Agnol Leite[1], Gabriel Luiz Montanhim[1], Leandro Fernandes[2], João Paulo Issa[3], Dimitrius Leonardo Pitol[3], Marcelo Carrijo da Costa[1], Gustavo Fernandes[1], Ariadne Rein[1], Rafael Scaf de Molon[4], Paola Castro Moraes[1]

[1]São Paulo State University "Júlio de Mesquita Filho", UNESP/FCAV-Jaboticabal, SP, Brasil
[2]São Paulo State University "Júlio de Mesquita Filho", UNESP/FOAr-Araraquara, SP, Brasil
[3]São Paulo University, Forp-USP, Ribeirão Preto, SP, Brasil
[4]São Paulo State University, Araçatuba School of Dentistry, SP, Brasil

Disclose and conflicts of interest: none to be declared by all authors

ABSTRACT

Introduction: the objective of this study was to compare the use of synthetic porous hydroxyapatite (SPH) with bovine xenograft (LB) to repair critical defects in the calvaria of Rattus novergicus, (Wistar lineage). Thirty-two adult rats were selected for the in vivo study and divided into four groups: negative control (absence of graft in the failure/blood clot); positive control (autograft); Lumina Bone (xenograft available on the market) and porous synthetic hydroxyapatite (test sub-stance). Surgical procedure was then performed on all rats, which were then analyzed through-out the postoperative period and randomly euthanized in two stages: at 6 weeks (n=4 – one rat from each group) for microtomography and at 12 weeks (n=28); 4 rats (one from each group) were chosen for microtomography, while the others were subjected to histopathological analysis. It was possible to observe bone growth and the percentage of collagen fiber distribution in sections stained with Masson's Trichrome and Picrosirius. Microtomographic analysis enabled the determination of volume to bone failure ratio. Thus, it may be concluded that PSH is a promising biomaterial, that facilitates intramembranous bone formation in the gaps, despite the need for further studies regarding its reabsorption and replacement.

Keywords: Ceramic Biomaterials; Bone graft; Bone Healing.

Introduction

For successful orthodontic and orthopedic surgeries, the interface between the implant and the bone must be mechanically stable. Extensive trauma with significant bone defects, either due to tumor excision or complex fractures, necessitates using grafts or biomaterials to provide bone stability[1].

The bone substitutes must have certain characteristics, named osteoconduction and osteoinduction. Biomaterial porosity is crucial for improved tissue formation[2,3]. Bone substitutes range from allogeneic, autogenous or xenogeneic grafts, there is also the use of biomaterials, it is important to highlight that the incorporation of these implants into a fracture occurs following the basic principles of fracture consolidation, which will be osseointegrated into the bone matrix through the action of osteoblasts and osteoclasts, also affected by the influence of numerous growth factors, mechanical stability and the location where they will be used[2,4], this action is mediated not only by the reabsorption capacity of the graft, but also by the osteogenic activity in the region[5].

Inflammation is the body's response to harmful stimuli that may come from infectious or non-infectious causes[6]. Once the inflammatory response is triggered, it occurs as a well-coordinated cascade of events, attracting inflammatory cells, such as macrophages, lymphocytes, granulocytes and plasma cells, to the site of tissue injury[7]. Macrophages that adhere to the surface of the biomaterial can fuse to form giant cells, which remain present throughout the implants remain in the host's body[8].

Lumina Bone® (Criteria, SP, Brazil) is a type of xenograft obtained from bovine bone; it has an osteoconductive structure that does not interfere with the osteoinductive factors of the patient's body. Lumina Bone is an organic biomaterial, whereas synthetic porous hydroxyapatite (SPH), studied in the present work, was developed using the sol–gel method[9], unlike Lumina Bone®, and is an active, synthetic ceramic biomaterial derived from calcium phosphate[10]. Its characteristics make it a useful biomaterial that accelerates host cell formation[11,12].

The present study aims to compare the bone repair abilities of SPH and Lumina Bone® in critical defects in the calvaria of *Rattus norvegicus*, Wistar lineage, through microtomographic and histopathological studies.

DOI: 10.51929/jms.43.114.2026
ISSN 2177-0298

Materials and Methods

Animals: The present study was conducted according to the ethical principles adopted by the National Council for the Control of Animal Experimentation and approved by the Committee on Ethics in the Use of Animals (CEUA) of the São Paulo State University (Unesp), School of Agricultural and Veterinarian Sciences, Jaboticabal (Protocol No. 4362/20).

The calvariums of 32 adult male rats (*Rattus norvegicus*, Wistar lineage) weighing an average of 300 g each were subjected to the creation of an 8 mm critical defect. The rats were subdivided into four groups according to the material used to cover the critical defect: C-: negative control (empty defect); C+: positive control (autogenous bone); LB: Lumina-Bone®; SPH: Porous Hydroxyapatite synthesized by the team. Each group consisted of eight rats, divided according to the following analysis times:

- A randomly selected rat destined for micro-CT in the 6th postoperative week;
- A randomly selected rat destined for micro-CT in the 12th postoperative week;
- Other rats in the group were sent for histopathological analysis in the 12th week after surgery.

Preparation of hydroxyapatite by the sol–gel method: One liter of a 0.5 mol/L solution of calcium hydroxide [$Ca(OH)_2$] and a liter of a 0.3 mol/L solution of phosphoric acid were prepared (H_3PO_4), keeping the Ca:P ratio = 1.67, according to the balanced chemical equation 1.

$$10Ca(OH)_2 + 6H_3PO_4 \xrightarrow{\text{(120; 300; 500; 700 e 800°C)}} 1Ca_{10}(PO_4)_6(OH)_2 + 18H_2O \quad (1)$$

The phosphoric acid solution was added to the calcium hydroxide solution, which underwent the process of aging, vacuum and dried at 60 °C for 12 hours, then the sample containing the powder was subjected to heat treatment at temperatures ranging from 100 to 800 °C for 3 hours. At a temperature of 700 °C it was possible to obtain the best results of specific surface area (SSE) of 160 $m^2.g^{-1}$, total porosity (TP) of 93.5% and an accumulated pore volume (APV) of 1.31 $mL.g^{-1}$, values that are higher than the world's leading material Bio-Oss®-Geistlish Switzerland and higher than the tested material from Lumina Bone (Critéria, Brazil) (Table 1).

Using 37 g of Ca(OH)2 and 20 mL of phosphoric acid (H3PO4), it is possible to synthesize approximately 50 g of HA. Therefore, there is a cost of BRL 0.035 per gram of material, without considering bureaucratic costs (taxes and costs of setting up a company at ANVISA) and operating expenses (person–hours, energy, packaging, water, electricity, etc.), which are extremely viable values.

Anesthetic and Surgical Procedures: The experiment was conducted according to the Manual of Care and Procedures with Laboratory Animals of the Vivarium of Production and Experimentation of FCF-IQ/USP[13]. The anesthetic protocol was standardized to use drugs of the same brand and batch in both groups. It consisted of the administration of ketamine 100 mg/ml (80 mg/kg/IP), xylazine 2% (5 mg/kg/IP), acepromazine 1% (1.5 mg/kg/IP), and morphine 10 mg/ml (1 mg/kg/IM). Half of the dose was administered before the procedure, and the other half during the thermal treatment.

A broad trichotomy of the entire cranial region of the animals was performed, followed by the application of 2% chlorhexidine and 70% alcohol antiseptic solutions; then definitive antisepsis was performed with 0.5% alcoholic chlorhexidine solution and preparation of the operative field. A 2-cm-long linear incision was made through the skin and subcutaneous tissue, extending from the interorbital region to the occipital region, using nº. 15 scalpel blades. The periosteum was incised, detached, and removed to expose the bone portions of the skull. A bone defect measuring 8 mm in diameter was mechanically created in this area using a trephine drill 8 mm in diameter (Neodent, Curitiba, PR, Brazil), taking care to maintain the integrity of the dura mater. The protocol for creating

Table 1. Physical chemical characteristics of natural bone, Bio-Oss®, Lumina bone® and SPH.

	Natural boné		Bio-Oss®[1]	Lumina one®[2]	SPH
	Cancellous Bone	Cortical Bone	-	-	-
Average particle size	*	*	250 - 1000 µm	300 - 425 µm	72 µm
Specific surface area	*	*	149 $m^2.g^{-1}$	57,888 $m^2.g^{-1}$	160 $m^2.g^{-1}$
Pore diameter	300-600 µm	10-50 µm	129,9 µm	111,9 µm	100 µm
Total porosity	*	*	89,6%	85%	93,5%
Accumulated pore volume	*	*	1,08 $mL.g^{-1}$	1,08 $mL.g^{-1}$	1,31 $mL.g^{-1}$
Ca/P	1,67	1,67	1,67	1,62	1,67

[1]Bio-Oss is a brand of the company Geistlich Holding.
[2]Lumina-Bone is a brand of the company Critéria Biomateriais.
*These parameters may vary according to species, weight and age[45].

the defect followed the technique proposed by Spicer *et al*. (2012)[14].

After perforation, the bone portion delimited by the diameter of the trephine drill was removed using a periosteal elevator. The bone defects were filled as per the protocol decided for each experimental group. The bone removed from the defect corresponding to the positive control (autogenous bone) was then ground with a gouge. The SPH experimental group had the defect filled with the SPH powder mixed in the blood present on the defect. The amount of biomaterial used was just enough to cover the area of the critical defect. After filling the bone defects, the subcutaneous tissue was approximated using a zigzag suture pattern with 4-0 nylon (Mononylon Ethicon, São Paulo, SP, Brazil), and the skin was sutured using the same material in a separate simple pattern.

After the procedure, the rats were housed in individual boxes positioned in the lateral recumbence position with the head higher, until they returned to consciousness. For 3 consecutive days, all animals received morphine at 1 mg/kg dose every 8 h.

Euthanasia: The euthanasia of the rats was performed at two different periods: the first in the 6th postoperative week of an animal randomly chosen from each group (destined for micro-CT) and the second in the 12th week of all animals (one animal for micro-CT and the others for histopathological analysis).

All animals were anesthetized using the same protocol as that used for surgery, followed by the intracardiac application of 5 mL of potassium chloride.

After the procedure, the defects were collected. The demarcated area was cut with a circular blade, and the collected samples were preserved in 4% paraformaldehyde in phosphate buffer for 48 h and then in 70% alcohol.

The samples used for micro-CT were preserved in 70% alcohol, whereas those intended for histopathological analysis were decalcified in 10% EDTA for 4 weeks and then preserved in 70% alcohol.

Computed microtomography (micro-CT) *ex vivo*: As proposed by Patel and collaborators (2008)[15] and Spicer *et al*. (2012)[14], micro-CT images of the areas of critical defects were captured for quantitative evaluation of bone repair.

The micro-CT analyses were performed using the Skyscan 1176 microtomograph (Aatselaar, Belgium, 2003 (Process 2009/54080-0 FAPESP - Multiuser Equipment Program 3) in the In Vivo Microtomography Laboratory of the Araraquara School of Dentistry, UNESP. After extracting the 2D and 3D images, the entire area of the defect was analyzed. The extension covered by the bone bridge (Fig. 1), which signals bone repair, was quantified according to the method proposed by Patel *et al*. (2008)[15], as described in table 2.

To obtain images with different parameters of micro-CT, the images were reconstructed using the NRecon software (SkyScan, 2011; version 1.6.6.0), oriented, and standardized according to three planes (transverse, longitudinal, and sagittal) through the Data Viewer software (SkyScan, version 1.4.4 64-bit). Then, using the CTAnalyser-CTAn software (2003-11SkyScan, 2012 Bruker Micro-CT Version 1.12.4.0), two regions of interest (ROIs) were determined using 2D images in the transaxial direction. After delimitation of the ROIs in the 2D images, bone volume analysis was performed on the 3D images using the collective sum of all ROIs, and the percentage of bone tissue volume present in each previously delimited area was obtained. Following the acquisition of the micrographic images, the classification of sample scores was carried out through blind analysis between observers, as the biomaterials used exhibit high radiopacity, making them easily distinguishable from the newly formed bone. No other segmentation was applied in the image editing software.

Histological Technique and Evaluation: The decalcified samples were embedded in paraffin and cut in semi-serial cuts of 5 µm in thickness, covering the entire calvaria. The sections were stained with Masson's trichrome, Picrosirius and Hematoxylin and Eosin to quantify new bone formation, differentiate type I and III collagen fibers and identify the cell types present in the gaps. Slide readings were performed using an optical microscope (AxioImager Z2; Zeiss, Germany) with a "motorized Z" stage coupled with a digital camera

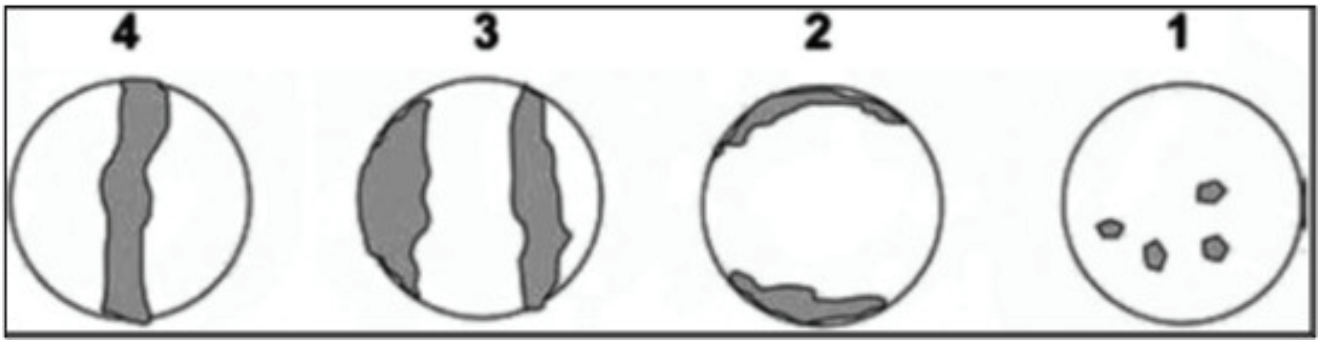

Figure 1. Schematic illustrations of the covering (gray) of the bone bridge formed in the bone defect in the calvaria of rats. The bone bridge score is mentioned above each illustration, as listed in Table 3. Image is taken from Patel *et al*. (2008)[15].

(Zeiss), allowing qualitative and quantitative in-depth analyses of the tissue.

Using the AxioImager Z2 optical microscope (Zeiss, Germany), coupled with a digital camera (Zeiss) and stereology techniques, the quantification of new bone formation (μm²) was performed in 16 random histological sections along the bone defect. The cuts were analyzed under the 10X objective of the microscope equipped with a "motorized Z" stage. For this quantification, the stereological software StérioInvestigator (MBF, USA) was used, which allows tissue volume analysis using the Cavalieri method, thus estimating new bone formation in 3D through the application of a test system composed of grids with a 150-μm distance over the contour of the area of interest. The results were obtained by employing the sum of points of the test system on the area of newly formed bone tissue demarcated, taking the thickness of 5 μm, as proposed by Issa *et al*. (2016)[16] and Gonzaga *et al*. (2019)[17].

Picrosirius staining allows visualization of type I and III collagen fibers through the birefringence of the fibers under a microscope with polarized light, which captures type I collagen fibers in a red/orange color and type III fibers in a green/yellow color[18]. Densitometric analysis was performed using the AxioVision program (Zeiss, Germany), which captures different shades of red and green light and quantifies the sum of the areas in pixels pertaining to the different fibers under polarized light. The area was expressed as the ratio of the collagen area to the total area and presented as a percentage.

Hematoxylin and eosin are a stain commonly used in laboratories to perform cellular differentiation. It is the basis for anatomopathological diagnosis, leading to the differentiation of cell types and tissues, providing information about the shapes, patterns and cellular structures of a sample. Hematoxylin stains acidic cellular components, such as nuclear chromatin, generating a deep blue purple or black color. Eosin stains cell cytoplasm, blood cells, collagen and muscles, giving the sample a shade of pink, demonstrating the "three-tone effect"[19]. Samples stained with HE were analyzed using optical microscopy to describe the findings.

Statistical Analysis: The results were analyzed using Kruskal-Wallis, Kenward-Roger, Analysis of Variance test (ANOVA) and Tukey test. P values < 0,05 were considered significant.

Results

Computed Microtomographic Assessment (micro-CT): After capturing the images, a 3D reconstruction was performed to further evaluate bone bridge formation (Fig. 1). The ratios between bone volume (BV) and total volume (TV) are shown in Figure 2. As TV is the total volume of the bone defect which includes bone and other tissues and BV is the amount of mineralized bone tissue within the gap, this ratio indicates the percentage of bone formed within the defect. A higher BV/TV ratio indicates a greater amount of bone relative to other tissues.

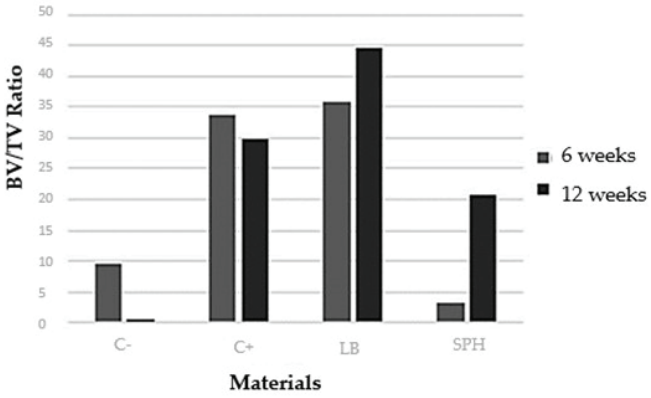

Figure 2. Ratio between bone volume and total volume of samples from the calvaria of Wistar strain rats with critical defect treated with negative and positive controls, Lumina Bone and Porous Synthetic Hydroxyapatite, respectively.

Microtomographic images of all groups are displayed in Figure 3, where it is possible to observe bone growth and the presence of xenografts and biomaterials in the gaps. According to the scores proposed by Patel and collaborators (2008)[15], as observed in Figure 1 and Table 2 the microtomographic images of Figure 3 were characterized as shown in Table 3. This characterization was made based on the BV/TV ratios as well as the subjective analysis of the images, considering the densities of both the newly formed bone and the biomaterial used.

Histopathological evaluation and statistical analysis: Twelve weeks postoperatively, the remaining animals were euthanized; therefore, each analyzed group contained five animals. The slides were 6 μm thick, with a spacing of 24 μm between the slices.

Masson's trichrome stain: Alternate sections were selected from each block, totaling 15 slides per block. Masson's trichrome staining allows the visualization of tissues in different colors. Nuclei are stained in black; elastic fibers, cytoplasm, keratin in red; and collagen in blue, as shown in Figure 4.

In the graph below (Fig. 5), the values found are the amount of bone formed within the critical flaw, it is possible to notice that only the C- group distances itself from the others, with a median area of 1645190 μm², while that C+, LB and SPH present very close values, 2340598, 2225342 and 2192164 μm², respectively. Both C+, LB and SPH present outliers, and a low amplitude of variance when compared to C-.

The Kruskall-Wallis analysis and subsequently, the Kenward-Roger test was performed, which, by ranking the groups, indicates which one presents statistical difference or not. It is possible to note that according to the Kenward-Roger test, there is no statistical difference between LB and C+ (A).

Picrosirius staining: For picrosirius staining, five

Table 2. Scores for bridge length and bone union using micro-CT datasets, adapted from Patel *et al*. (2008)[15].

Description of the Score Bone Bridge	Score
Bone bridge covering the entire length of the defect at the longest point (08 mm)	4
Bone bridge over the partial length of the defect	3
Bone bridge only at the edge of the defects	2
Few bone spicules dispersed throughout the defect	1
No bone formation in the defect	0

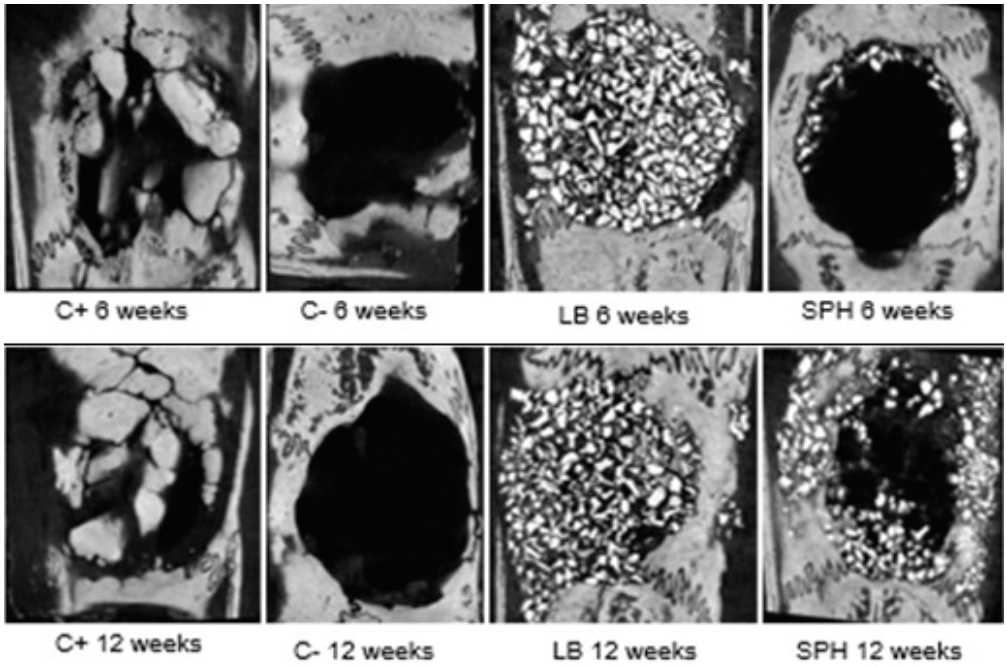

Figure 3. Microtomography scan of groups C+ (positive control), C- (negative control), LB (Lumina Bone) e SPH (synthetic porous hydroxyapatite) at 6 and 12 weeks.

Table 3. Classification according to scores by Patel *et al*. (2008), correlated with the microtomography images found in the present study.

Samples	Score	
C- 12 weeks	Score 0 No bone formation in the defect.	
C- 6 weeks C+ 6 weeks LB 6 weeks SPH 6 weeks	Score 2 Bone bridge only ate the edge of the defects	
LB 12 weeks	Score 3 Bone bridge over partial length of defect	
C+ 12 weeks SPH 12 weeks	Score 4 Bone bridge covering the entire length of the defect at the longest point (08 mm)	

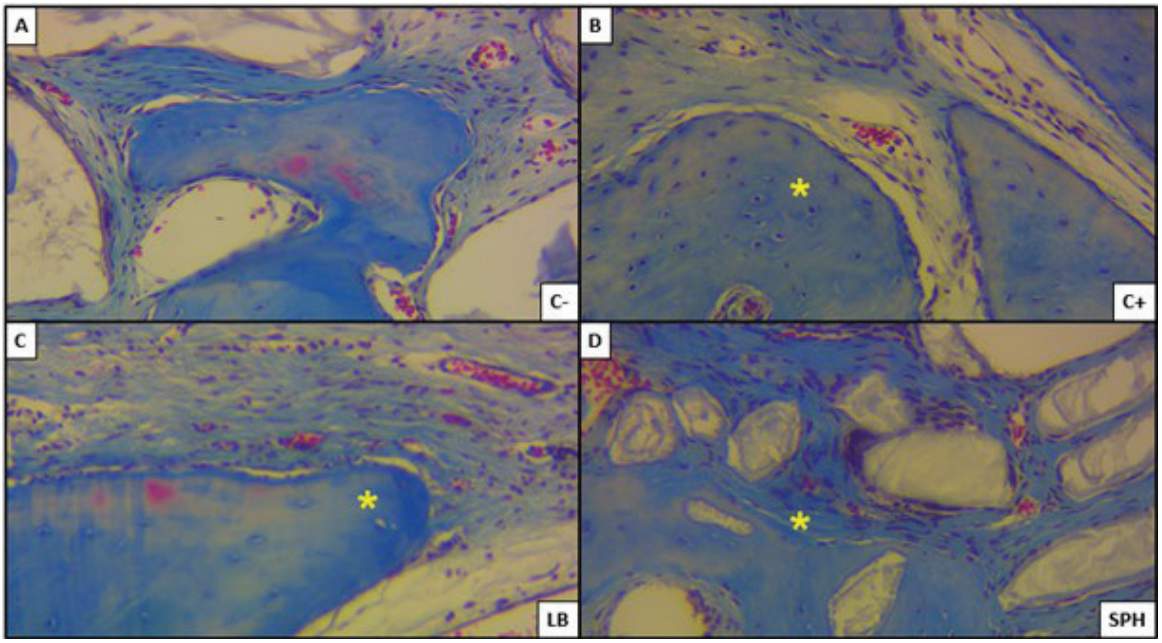

Figure 4. Photomicrographs of the calvaria of Wistar strain rats, with critical defect, treated with: A - empty defect, B - Autograft, C - Lumina Bone, and D - Porous Synthetic Hydroxyapatite at 12 weeks postoperatively. Staining: Masson's trichrome. Yellow asterisks: bone bridge formation.

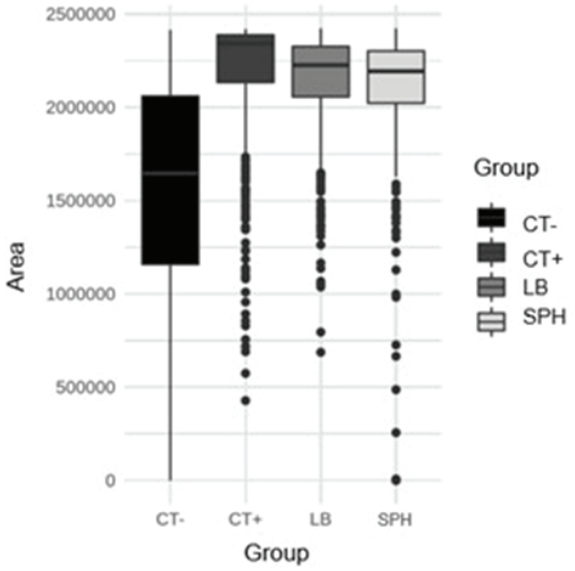

Figure 5. Boxplot graph showing the medians, range and outliers of each treatment with Masson's Trichrome.

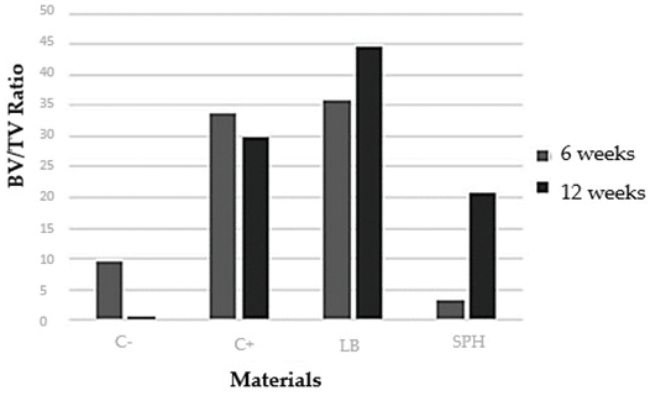

Figure 6. Photomicrographs of the calvaria of Wistar strain rats, with critical defect, treated with: A - empty defect, B - Autograft, C - Lumina Bone, and D - Porous Synthetic Hydroxyapatite at 12 weeks postoperatively. Treatment with Picrosirius staining makes it possible to visualize Type I (white arrow) and Type III (blue arrow) collagen fibers.

slides of each block were selected in which the edges of the defects were analyzed to quantify total collagen. The color indicated collagen fibers when observed under polarized light; type I collagen fibers appeared reddish-orange and type III appeared yellow-green (Fig. 6). All slides were photographed and analyzed in the Image J program to assess the total area of collagen.

In the boxplot type graph (Fig. 7) for analysis of treatments with picrosirius, the median was also evaluated, but this time with the percentage of collagen area within the defects. Thus, the medians of C-, C+, LB and SPH are respectively: 25.764%, 28.2805%, 27.9350% and 29.3220%, the group that presented the most outliers were the SPH and the one with the greatest variation in amplitude was LB.

For the evaluation of slides stained with picrosirius, a total of 482 observations were used: 140, 104, 124 and 114, respectively for C-, C+, LB, SPH. Here, the percentage of collagen per photomicrograph area was analyzed.

The variance analysis test (ANOVA) was applied, the H0 was rejected (because at least one group differs), significance level 5%, therefore, the Tukey test was applied.

With the evaluation of the mean values, 2 to 2, through Tukey's test, it was possible to observe that the C- group presented a difference only in SPH. C+ differed from both LB and SPH, but not from C-. The LB

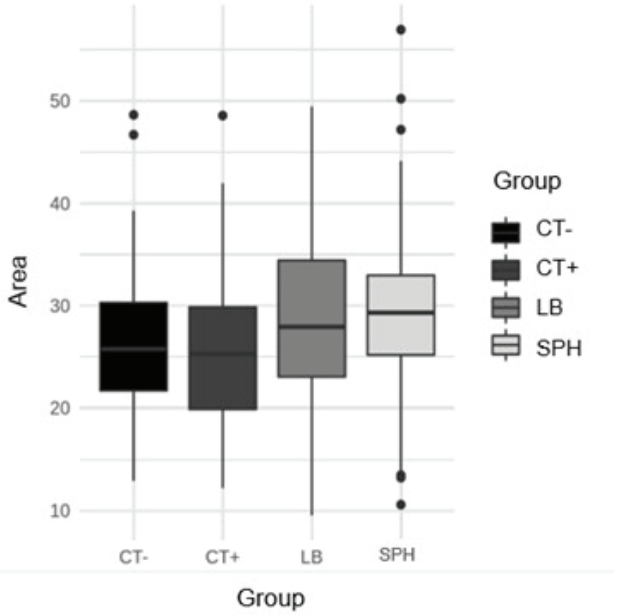

Figure 7. Boxplot graph showing the medians, range and outliers of each Picrosirius treatment.

group showed no difference in C- and SPH, finally, the SPH group (a) was significantly different from C- (bc) and C+ (c), but not from LB (ab).

Hematoxylin and eosin staining: For HE staining, one slide of each block was selected in which the edges of the defects were analyzed using optical microscopy to describe and identify the cell types present in the gaps (Fig. 8 and Fig. 9).

Microscopic analysis: A – Negative control, 4x: Sparse bone tissue, with a predominance of fibrous connective tissue at the site of the defect. Absence of formed bone trabeculae or expected regenerative activity.

a– Negative control, 10x: Presence of disorganized connective tissue. There are no signs of new bone matrix deposition or evident osteoblastic activity.

B– Positive control, 4x: Evidence of bone formation around a defect characterized by areas with developing bone trabeculae. Possible vascularization in intertrabecular areas.

b– Positive control, 10x: Osteoblasts aligned on the surface of the trabeculae, indicating

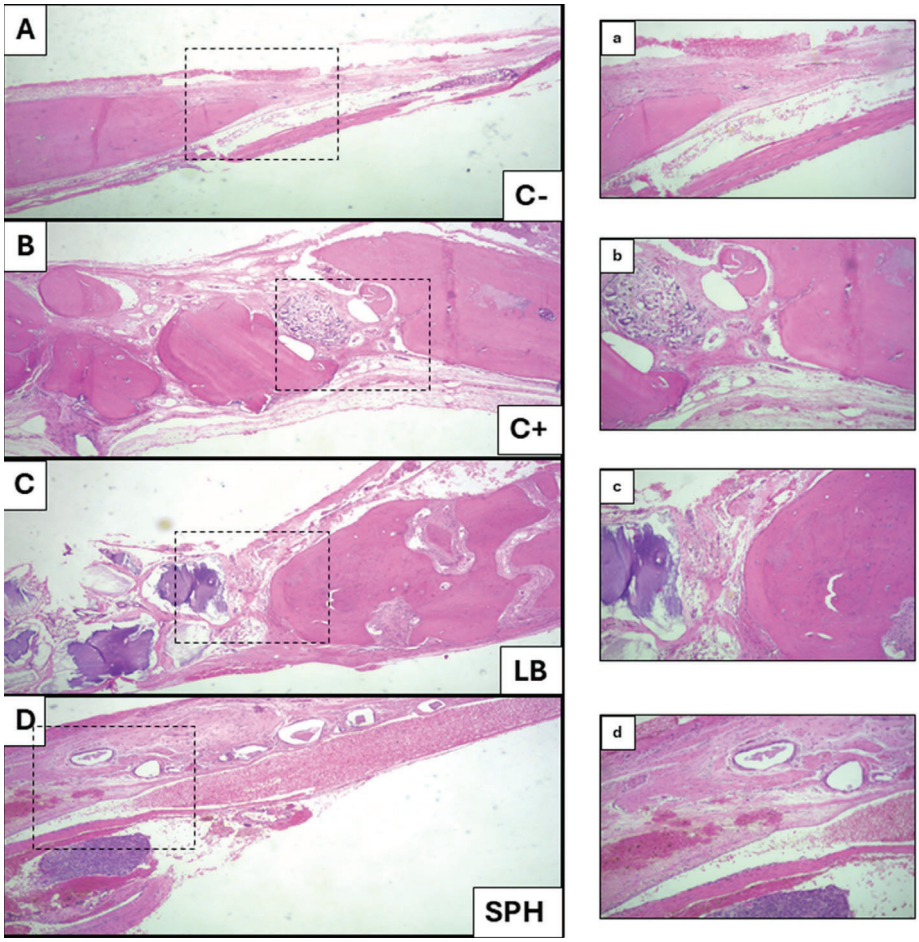

Figure 8. Photomicrographs of the calvaria of Wistar strain rats, with critical defect, treated with A - empty defect 4x, B – Autograft 4x, C - Lumina Bone 4x, D - Porous Synthetic Hydroxyapatite 4x, a - empty defect 10x with presence of disorganized connective tissue (red asterisk), b – Autograft 10x with presence of bone trabeculae and vascularization (black and green asterisks respectively), c - Lumina Bone 10x with presence of bone trabeculae, connective tissue and particles of lumina bone (black, red and orange asterisks respectively), and d - Porous Synthetic Hydroxyapatite 10x with presence of bone trabeculae, vascularization and particles of SPH (black, red and blue asterisks respectively) at 12 weeks postoperatively. Treatment with HE staining makes it possible to visualize all the cell types involved in bone consolidation.

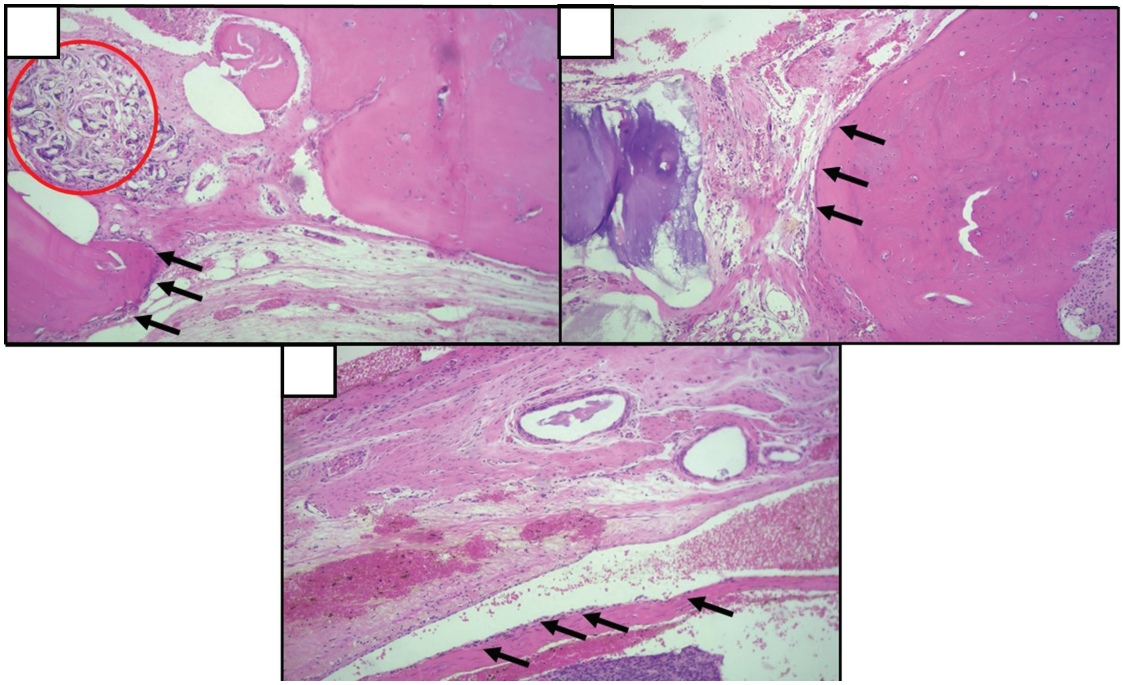

Figure 9. Photomicrographs of the calvaria of Wistar strain rats, with critical defect, treated with b – Autograft 10x with presence of Osteoblasts and mononuclear inflammatory infiltrate (black arrow and red circle, respectively), c - Lumina Bone 10x with presence of Osteoblasts (black arrow), and d - Porous Synthetic Hydroxyapatite 10x with presence of Osteoblasts (black arrow) at 12 weeks postoperatively. Treatment with HE staining makes it possible to visualize all the cell types involved in bone consolidation.

osteogenic activity. Gaps containing osteocytes are visible within the trabeculae, characterizing developing lamellar bone. Presence of mononuclear inflammatory infiltrate composed of macrophages, giant cells and lymphocytes.

C- Lumina Bone, 4x: Evident presence of grafted material with basophilic color suggesting remaining particles of the graft. Intertrabecular spaces filled with vascularized connective tissue.

c- Lumina Bone, 10x: Areas of osteogenesis surrounded by active osteoblasts. Lamellar bone formation with the presence of multinucleated giant cells around the graft particles suggesting controlled resorption and integration of the graft.

D- Porous Synthetic Hydroxyapatite, 4x: Evidence of hydroxyapatite particles at the defect site showing dense eosinophilic and homogeneous coloration. Formation of immature bone tissue around the particles with bone trabeculae in formation acting as osteoconductive support. Presence of connective tissue and moderate vascularization.

d- Porous Synthetic Hydroxyapatite, 10x: Hydroxyapatite particles in the process of resorption with the formation of bone trabeculae. Presence of localized areas showing active osteoblasts. Predominant vascularized connective tissue in areas further away from the grafted material.

Discussion

In general, the bone repair process manages to reestablish the cell composition, structure and biomechanical function pre-trauma, but in addition to critical failures, which are characterized by not regenerating sufficiently to bridge the width of the defect, about than 10% of fractures may not regenerate properly[20], so it is necessary to use adjuvants for their reconstruction, such as biomaterials or grafts, even though in veterinary medicine autologous bone is still the most viable option, the use of biomaterials has been rising in the last two decades, whether as an experimental model or attempts to save limbs in extensive bone loss[21,22,23].

The xenografts made from bovine bone tissue are classified as osteoconductive, in this way they allow bone growth on their surface, they present slow reabsorption and degradation[24,25]. The material used in the LB group, according to the manufacturer's information, has a surface area of 57,888 $m^2.g^{-1}$, with a Ca/P ratio of 1.62 and micropores of 111.9 µm. The SPH sample used in the present study has a surface area of 160$m^2.g^{-1}$, being quite greater than the area of the LB which facilitates the adhesion of bone cells, in relation to the pores, according to Werner [26], pores above 100 µm facilitate bone neoformation, migration and cell transport, both biomaterials present pores within this range. The Ca/P ratio was slightly lower than the theoretical hydroxyapatite Ca/P = 1.67 for the LB material (1.62) and identical for the SPH (1.67). The higher the ratio, the lower the solubility and the more crystalline the material, both key factors for material absorption and new bone formation[27].

There are many reports on how the particle size of a biomaterial can interfere with the quality of newly formed bone, accelerating resorption and remodeling rates, with the vast majority of researchers considering that the ideal particle size varies from 100 to 300 μm[28,29,30,31], in this study, the SPH used had an average particular size of 72 μm, while the LB had an average size of 300 to 425 μm, which may explain the statistical difference found between the groups evaluated regarding the amount of newly formed bone within the defect, without there being a significant statistical difference in collagen formation between the SPH and LB groups, since LB, being a biomaterial originating from the mineral part of bovine bone, produces greater local inflammatory reaction, leading to greater cell proliferation and consequently promoting a better environment for bone growth, as can be seen in images with HE staining[32].

A non-destructive way to verify the viability of these new materials and the way they behave in bone repair in experimental studies is through the use of micro-CT, in the present study they were performed during the period of 6 and 12 weeks after surgery, where it was observed that the group treated with SPH presented a BV/TB ratio of 2.95% after 6 weeks, but this may be due to a possible absorption that hydroxyapatite undergoes during this period, mediated by osteoclasts, this absorption is controversial, despite being excellent osteoconductor and osseointegrator, it presents low biodegradation[33], as was observed in the present study, because at the end of the experiment, both in histological and microtomographic images it is possible to show the presence of biomaterial particles surrounded by connective tissue, since some studies demonstrate that it may vary according to the size of the biomaterial, the porosity and the temperature at which it was synthesized[34], which helps to explain why the SPH 12 week group was classified as score 4, since they were classified according to the score through blind analyzes between observers.

All groups evaluated at 6 weeks had better results in filling the gap when compared to the C- group, except for the SPH group, this is probably due to the material itself, since hydroxyapatite needs further studies regarding its ability to be absorbed, as already mentioned. And on the other hand, the difference of only 8.54% between the BV/TV ratio at 6 and 12 weeks demonstrated in the LB group is probably due to the fact that xenografts from the inorganic part of bovine trabecular bone act as a support for the growth of cells within its pores, inertly[35].

In the 12-week period, a considerable increase was observed for the same ratio in the SPH group, reaching 20.53%, coming close to the value found in the C+ group, which presented 29.68%. It is known that the autograft is still considered the gold standard for the treatment of this type of injury, due to its properties of osteoinduction, osteoconduction and osseointegration[22], in this present study the autograft used was from lamellar bone, this has mesenchymal origin, which causes an intramembranous type ossification to occur, this bone type also has immunological properties that generate resistance to absorption[36], which may explain the little difference between the ratios at 6 and 12 weeks in the C+ group.

However, at 12 weeks of experiment, including the group treated with SPH, it showed better filling of the gap than the C- group, as evidenced in the work of Patel[15], in which the experimental groups also showed better results than the negative control, thus highlighting the need to use adjuvants in the treatment of critical defects, as there is no support structure for bone matrix deposition.

Unfortunately, the analysis conducted with the aid of micro-CT delivers the total volume of the filling of the defect, including remnants of the graft that may be present. For the analysis to be more reliable, demonstrating the volume of newly formed bone, the histopathological evaluation was carried out at the end of the 12 weeks of the experiment, the results were consistent with those obtained through micro-CT.

As already described the histological sections stained with Masson's Trichrome stain, was evaluated about the formation of bone tissue, the C+ and LB groups did not show statistical difference when their areas were compared using the Keward-Roger test, but when the behavior of their areas were graphically examined together with the SPH group, it was possible to observe that their medians were very close, leading to believe that SPH acted as a good osteoinductor, as in the work by Lin *et al.* (2009)[37], Habibovic *et al.* (2005)[38], although it is not clear how this occurs, and it involves many factors of the bone microenvironment that were not evaluated in the present study, one must take into account its physical characteristics, such as porosity, surface area, topography and geometry.

In the slides stained with picrosirius staining, it was possible to evaluate the percentage of collagen present in the defects as demonstrated in the study by Padilla and collaborators (2021)[39], picrosirius is an excellent staining for qualitative and quantitative analyzes of collagen, but for differentiating types of collagen is not very effective, Liu *et al.* (2021)[40] take into account the fact that microscopic analyzes are two-dimensional evaluations, which can lead to errors in the evaluation of something as complex as collagen fibers that have a three-dimensional structure, but some studies used this staining to perform this differentiation, so that when observing the image of the slide by microscopy, the reddish fibers are already matured type I collagen, those stained in yellow are also type I collagen, but in maturation process and the green ones are collagen type III[41,42,43,44]. Such differentiation was not used in the present study.

Even so, it was possible to note that even the C- group did not present such expressive measures in

bone growth at 12 weeks, both in the micro-CT analysis and in the slides stained with Masson's Trichrome, it presented an average of the percentage of collagen superior to the C+ and equal to the LB experimental group, being inferior only to the SPH group, possibly because collagen is a type of tissue architecture marker and the use of hydroxyapatite in conjunction with implants makes the adhesion of the latter to occur in an easier way and with more accelerated bone neoformation[42].

It is known that the search for low-cost biomaterials that help in bone repair, both in human and veterinary medicine, is continuous[22], especially when submitting the patient to other surgical procedures for the acquisition of autografts can generate more complications, due to the increase in surgical time and new incision sites. Thinking about xenografts, considering the results obtained here regarding the use of SPH, a comparison can be made based on the value of the materials. The present biomaterial tested here is 8400 times cheaper than the xenograft used in the LB group, which would allow its more frequent use and with greater reach among professionals working in the area.

Conclusion

It was possible to conclude that after 12 weeks of experiment, the SPH group had comparable bone formation to the autograft group, with extensive bridging of the defect. From the morphological point of view, it showed good collagen deposition, which is used as support for bone growth, leading to good osteoconduction and osteoinduction, and consequently to bone formation in critical failures, not exhibiting a foreign body reaction. The negative control group showed extraordinarily little bone formation. However, this was a short-term study demonstrating the promising potential of SPH for bone reconstruction, so further studies are needed for long-term evaluation, especially regarding its rate of resorption and replacement. With additional characterization and testing, SPH could become a viable bone graft alternative.

Acknowledgments

To CNPq (Conselho Nacional de Desenvolvimento Científico e Tecnológico), for the scholarship and financial support that enabled full dedication to the graduate program and operationalization of the study.

References

1. Rolvien T, Barvencik F, Klatte TO, Busse B, Hahn M, Rueger JM, *et al*. ß-TCP bone substitutes in tibial plateau depression fractures. Knee. 2017 Oct 1;24(5):1138–45. Available in: https://doi.org/10.1016/j.knee.2017.06.010.

2. Bose S, Vahabzadeh S, Bandyopadhyay A. Bone tissue engineering using 3D printing. Vol. 16, Materials Today. 2013. p. 496–504. Available in: https://doi.org/10.1016/j.mattod.2013.11.017

3. Rolvien T, Barbeck M, Wenisch S, Amling M, Krause M. Cellular mechanisms responsible for success and failure of bone substitute materials. v. 19, International Journal of Molecular Sciences. MDPI ago. 2018. Available in: https://doi.org/10.3390/ijms19102893

4. Schilling A F, Linhart W, Filke S, Gebauer M, Schinke T, Rueger J M, Amling M. Resorbability of bone substitute biomaterials by human osteoclasts. Biomaterials, v. 25, n. 18, p. 3963–3972, ago. 2004. Available in: https://pubmed.ncbi.nlm.nih.gov/15046886/

5. Draenert M, Draenert A, Draenert K. Osseointegration of hydroxyapatite and remodeling-resorption of Tricalciumphosphate Ceramics. Microscopy Research and Technique 76(4) p. 370-380. apr. 2013. Available In: https://pubmed.ncbi.nlm.nih.gov/23390042/.

6. Medzhitov, R. Inflammation 2010: New Adventures of an Old Flame. Cell, [s. l.], v. 140, n. 6, p. 771–776, 2010. Available in: https://pubmed.ncbi.nlm.nih.gov/20303867/

7. Chen, L.; Deng, H.; Cui, H, *et al*. Oncotarget. www.impactjournals.com/oncotarget Inflammatory responses andinflammation-associated diseases in organs. Oncotarget, [s. l.], v. 9, n. 6, p. 7204–7218, 2018. Available in: https://www.ncbi.nlm.nih.gov/pmc/articles/PMC5805548/

8. Anderson, J. M. Exploiting the inflammatory response on biomaterials research and development. Journal of Materials Science: Materials in Medicine, [s. l.], v. 26, n. 3, 2015. Available in: https://pubmed.ncbi.nlm.nih.gov/25690617/

9. Costa ACFM, Lima M G, Lima LHMA, Cordeiro VV, Viana KMS, Souza CV, *et al*. Hidroxiapatita: Obtenção, caracterização e aplicações. 2009 Available in: www.dema.ufcg.edu.br/revista

10. Dorozhkin S V. Calcium orthophosphates in nature, biology and medicine. Vol. 2, Materials. MDPI AG; 2009. p. 399–498. Available in: https://doi.org/10.3390/ma2020399.

11. Amini AR, Adams DJ, Laurencin CT, Nukavarapu SP. Optimally porous and biomechanically compatible scaffolds for large-area bone regeneration. Tissue Eng Part A. 2012 Jul 1;18(13–14):1376–88. Available in: https://doi.org/10.1089/ten.tea.2011.0076.

12. Brown BN, Ratner BD, Goodman SB, Amar S, Badylak SF. Macrophage polarization: An opportunity for improved outcomes in biomaterials and regenerative medicine. Biomaterials. v. 33, (2012) p. 3792–3802. Available in: https://doi.org/10.1016/j.biomaterials.2012.02.034.

13. Du Sert NP, Hurst V, Ahluwalia A, Alam S, Avey MT, Baker M, *et al*. The ARRIVE guidelines 2.0: Updated guidelines for reporting animal research. 2020. Available in: https://doi.org/10.1371/journal.pbio.3000410.

14. Spicer PP, Kretlow JD, Young S, Jansen JA, Kasper FK, Mikos AG. Evaluation of bone regeneration using the rat critical size calvarial defect. Nat Protoc. 2012 Sep 6;7(10):1918–29. Available in: https://doi.org/10.1038/nprot.2012.113.

15. Patel ZS, Young S, Tabata Y, Jansen JA, Wong MEK, Mikos AG. Dual delivery of an angiogenic and an osteogenic growth factor for bone regeneration in a critical size defect model. Bone. 2008;(43)931–40. Available in: https://pubmed.ncbi.nlm.nih.gov/18675385/.

16. Issa JP, Gonzaga M, Kotake BG, De Lucia C, Ervolino E, Iyomasa M. Bone repair of critical size defects treated with autogenic, allogenic, or xenogenic bone grafts alone or in combination with rh BMP-2. Clin Oral Impl Research, 27(5), (2016) 558-566. Available in: https://doi.org/ 10.1111/clr.12622.

17. Gonzaga MG, dos Santos Kotake BG, de Figueiredo FAT, Feldman S, Ervolino E, dos Santos MCG, *et al*. Effectiveness of rhBMP-2 association to autogenous, allogeneic, and heterologous bone grafts. Microsc Res Tech. 2019 Jun 1;82(6):689–95. Available in: https://doi.org/10.1002/jemt.23215.

18. Cury DP, Dias FJ, Miglino MA, Watanabe IS. Structural and ultrastructural characteristics of bone-tendon junction of the calcaneal tendon of adult and elderly Wistar rats. PLoS One, 2016, 11: e0153568. Available in: https://doi.org/10.1371/journal.pone.0153568.

19. Feldman AT, Wolf D. Tissue Processing and Hematoxylin and Eosin Staining. In: Day, C. Histopathology. Methods in Molecular Biology.

New York: Humana Press. vol. 1180. cap. 3, p. 31-43. 2014.
20. Zhu G, Zhang T, Chen M, Yao K, Huang X, Zhang B, *et al*. Bone physiological microenvironment and healing mechanism: Basis for future bone-tissue engineering scaffolds. Vol. 6, Bioactive Materials. KeAi Communications Co.; 2021. p. 4110–40. Available in: https://doi.org/10.1016/j.bioactmat.2021.03.043.
21. Campos JM, Sousa AC, Pinto PO, Ribeiro J, França ML, Caseiro AR, *et al*. Application of Bonelike® as synthetic bone graft in orthopaedic and oral surgery in veterinary clinical cases. Biomater Res. 2018 Dec 29;22(1). Available in: https://doi.org/10.1186/s40824-018-0150-x.
22. Galia CR, Moreira LF. The Biology of Bone Grafts. 2012. In: Galia CR, Moreira LF. Recent Advances in Arthroplasty. InTech. pp. 235-251. Available in: https://doi.org/10.5772/27381
23. Pinto PO, Branquinho M V., Caseiro AR, Sousa AC, Brandão A, Pedrosa SS, *et al*. The application of Bonelike® Poro as a synthetic bone substitute for the management of critical-sized bone defects - A comparative approach to the autograft technique - A preliminary study. Bone Rep. 2021 Jun 1;14. Available in: https://doi.org/10.1016/j.bonr.2021.101064
24. Calasans-Maia MD, Resende R, Fernandes G, Calasans-Maia J, Alves AT, Granjeiro JM. A randomized controlled clinical trial to evaluate a new xenograft for alveolar socket preservation. Clin. Oral Impl. Res. 2013. Available in: https://doi.org/10.1111/clr.12237.
25. Calasans-Maia MD, Rossi AM, Dias EP, Santos SRA, Áscoli F, Granjeiro JM. Stimulatory Effect on Osseous Repair of Zinc Substituted Hydroxyapatite: Histological Study in Rabbit's Tibia. Key Eng Mater. 361-363: 1269-1272, 2008. Available in: https://doi.org/10.4028/www.scientific.net/KEM.361-363.1269
26. Werner J, Linner-Krcmar B, Friess W, Greil P. Mechanical properties and in vitro cell compatibility of hydroxyapatite ceramics with graded pore structure. Vol. 23, Biomaterials. 2002. Available in: https://doi.org/ 10.1016/s0142-9612(02)00191-6.
27. Silva AN, Sartoretto CS, Ferreira Barreto-Vieira D, Mauro Granjeiro J, Diuana Calasans-Maia M. Caracterização físico-química de três xenoenxertos utilizados na implantodontia Physicochemical characterization of three xenografts used in implant dentistry [Internet]. 2020. Available in: https://doi.org/10.22409/ijosd.v0i54.40997
28. Rivault AF, Toto PD, Levy S, Gargiulo AW. Autogenous bone grafts: osseous coagulum and osseous retrograde procedures in primates. Vol. 42, Journal of Periodontology; 1971. p. 787–796. Available in: https://doi.org/10.1902/jop.1971.42.12.787
29. Shapoff CA, Bowers GM, Levy B, Mellonig JT, Yukna RA. The effect of particle size on the osteogenic activity of composite grafts of allogenic freeze-dried bone and autogenous marrow. Vol. 51, Journal of Periodontology; 1980. p. 625–630. Available in: https://doi.org/10.1902/jop.1980.51.11.625
30. Hall EE, Meffert RM, Hermann JS, Mellonig JT, Cochran DL. Comparison of bioactive glass to demineralized freeze-dried bone allograft in the treatment of intrabony defects around implants in the canine mandible. Vol. 70, J Periodontology; 1999. p. 526–535. Available in: https://doi.org/10.1902/jop.1999.70.5.526
31. Pallesen L, Schou S, Aaboe M, Hjørting-Hansen E, Nattestad A, Melsen F. Influence of particle size of autogenous bone grafts on the early stages of bone regeneration: a histologic and stereologic study in rabbit calvarium. Vol 17, International Journal of Oral & Maxillofacial Implants; 2002. p. 498–506. Available in: PMID: 12182292.
32. Figueiredo AS, Fagundes DJ, Novo NF, Inouye CM, Takita LC, Sassioto MCP. Osteointegração de osso bovino desvitalizado, hidroxiapatita de coral, poliuretana de mamona e enxerto autógeno em coelhos. Vol 19, Acta Cirúrgica Barsileira; 2004. p. 370–382. Available in: https://doi.org/10.1590/S0102-86502004000400008
33. Kumar A, Kargozar S, Baino F, Han SS. Additive Manufacturing Methods for Producing Hydroxyapatite and Hydroxyapatite-Based Composite Scaffolds: A Review. Vol. 6, Frontiers in Materials; 2019. Front mater. Available in: https://doi.org/10.3389/fmats.2019.00313
34. Goto T, Kojima T, Iijima T, Yokokura S, Kawano H, Yamamoto A, Matsuda K. Resorption of synthetic porous hydroxyapatite and replacement by newly formed bone. J Orthop Sci (2001) 6:444–447. Available in: https://doi.org/10.1007/s007760170013.
35. Munhoz EA, Bodanezi A, Cestari TM, Graeff MSZ, Ferreira O, De Carvalho PSP, *et al*. Impact of inorganic xenograft on bone healing and osseointegration: An experimental study in rabbits. Implant Dent. 2017 Dec 1;26(6):875–81. Available in: https://doi.org/10.1097/ID.0000000000000694.
36. Macedo A, Lamelo SG, Alencar E, Caballero F, Gimenes E, Zubieta C. Enxerto ósseo em crânio: princípios básicos para a integração óssea. Rev. Bras. Cir. Plást. 2010; 25(4): 617-23. Available in: https://doi.org/10.1590/S1983-51752010000400009
37. Lin L, Chow KL, Leng Y. Study of hydroxyapatite osteoinductivity with an osteogenic differentiation of mesenchymal stem cells. J Biomed Mater Res A. 2009 May;89(2):326–35. Available in: https://doi.org/10.1002/jbm.a.31994.
38. Habibovic P, Yuan H, Van der Valk CM, Meijer G, Van Blitterswijk CA, de Groot K. 3D microenvironment as essential element for osteoinduction by bio¬materials. Biomat. (2005) 26:3565–3575. Available in: https://doi.org/ 10.1016/j.biomaterials.2004.09.056.
39. López De Padilla CM, Coenen MJ, Tovar A, De la Vega RE, Evans CH, Müller SA. Picrosirius Red Staining: Revisiting Its Application to the Qualitative and Quantitative Assessment of Collagen Type I and Type III in Tendon. Journal of Histochemistry and Cytochemistry. 2021 Oct 1;69(10):633–43. Available in: https://doi.org/ 10.1369/00221554211046777.
40. Liu J, Xu M you, Wu J, Zhang H, Yang L, Lun D xing, *et al*. Picrosirius-Polarization Method for Collagen Fiber Detection in Tendons: A Mini-Review. Vol. 13, Orthopaedic Surgery. Sociedade Brasileira de Matematica Aplicada e Computacional; 2021. p. 701–7. Available in: https://doi.org/ 10.1111/os.12627.
41. Dziedzic-Goclawska A, Rozycka M, Czyba JC, Moutier R, Lenczowski S, Ostrowski K. Polarizing microscopy of Picrosirius stained bone sections as a method for analysis of spatial distribution of collagen fibers by optical diffractometry. Basic Appl Histochem. 1982;26(4):227-39. Available in: https://pubmed.ncbi.nlm.nih.gov/6187326/.
42. Allegrini, E. Rumpel, E. Kauschke, J. Fanghänel, B. König. Hydroxyapatite grafting promotes new bone formation and osseointegration of smooth titanium implants. Annals of Anatomy 188 (2005) 143–151. Available in: https://doi.org/10.1016/j.aanat.2005.08.019.
43. Junqueira LC, Carneiro J. Tecido ósseo. In: JUNQUEIRA, L. C; CARNEIRO, J. Histologia básica. 12. ed. Rio de Janeiro: Guanabara koogan. cap. 8, p. 131-148. 2013.
44. Gupta S, Aggarwal R, Gupta V, Vij R, Tyagi N, Misra A. Picrosirius red: A better polarizing stain J of Histotech 40 (2017) 46–53. Available in: http://dx.doi.org/10.1080/01478885.2017.1325111
45. Lerebours C, Thomas C D L, Clement J G, Buenzli P R, Pivonka P. The relationship between porosity and specific surface in human cortical bone is subject specific. Bone. 2015 Mar:72:109-17. Available in: https://pubmed.ncbi.nlm.nih.gov/25433340/

Mini Curriculum and Author's Contribution

1. Marcella Dall Agnol Leite - DVM; MSc. Contribution: Conceptualization, Methodology, Formal analysis, Investigation, Data curation, Writing-original draft, review and editing.

2. Gabriel Luiz Montanhim - DVM; PhD. Contribution: Conceptualization, Methodology, Formal analysis, Investigation, Data curation.

3. Leandro Fernandes - PhD. Contribution: Resources ORCID: 0009-0000-9555-0053

4. João Paulo Mardegan Issa - PhD. Contribution: Conceptualization, Supervision. ORCID: 0000-0002-1056-0795 0000-0002-1056-0795

5. Dimitrius Leonardo Pitol - PhD. Contribution: Conceptualization, Methodology, Supervision. ORCID: 0000-0001-5943-2359

6. Marcelo Carrijo da Costa - DVM; PhD. Contribution: Data curation. ORCID: 0000-0003-4014-4351

7. Gustavo Fernandes - DVM; MSc. Contribution: Data curation. ORCID: 0000-0001-5410-476X

8. Ariadne Rein - DVM; MSc, Contribution: Data curation. ORCID: 0000-0003-0181-6768

9. Rafael Scaf de Molon - PhD. Contribution: Data curation. ORCID: 0000-0003-1110-6233

10. Paola Castro Moraes - DVM; PhD. Contribution: Conceptualization, Methodology, Supervision, Project administration. ORCID: 0000-0002-0255-2971

Received: February 2, 2026
Accepted: July 2, 2026

Corresponding author
: Marcella Dall Agnol Leite
E-mail: dallagvet@gmail.com